Chemical Mechanism of the $Zr + O_2 \rightarrow ZrO_2$ Combustion Synthesis Reaction

M. Arimondi,[†] U. Anselmi-Tamburini,[†] A. Gobetti,[‡] Z. A. Munir,[§] and G. Spinolo*,[†]

Department of Physical Chemistry, INCM, and C.S.T.E./CNR, University of Pavia, I 27100-Pavia, Italy, Department of Structural Mechanics, University of Pavia, I 27100-Pavia, Italy, and Division of Materials Science and Engineering, University of California, Davis, California 95616

Received: November 26, 1996; In Final Form: June 23, 1997[⊗]

The oxidation of Zr particles under a combustion regime is investigated by discussing separately the macrokinetic aspects (Fourier's law of heat transfer) and the microkinetic aspects (the kinetic laws describing chemical and phase transformations of a solid particle). A very simple model with a single reaction step and two different mechanisms (and different laws) is assumed to describe the microkinetics, while filtration of the gaseous reagent through the porous sample is neglected. The microkinetic variables (conversion degree and temperature) are then identified with the corresponding global variables, and the set of macrokinetic equations is finally solved by numerical methods. The approach is used to investigate how the *chemical* mechanism is affected by process parameters such as oxygen partial pressure, size of the reacting particles, and dilution degree. It is shown that experimental determinations (such as wave speed, thermal and composition profiles, and their dependence on process parameters) can be effectively used to clarify the chemical mechanism of the combustion. Improvements of the approach and extensions to multistep reactions are also discussed.

1. Introduction

Self-propagating high-temperature synthesis (SHS), or combustion synthesis, is an alternative synthetic method for producing a wide class of simple and complex inorganic materials having high chemical purity and excellent physical and mechanical properties. The method is based on the ability of an exothermic heterogeneous chemical reaction to become self-sustaining and propagate as a combustion wave through the mixture of the reactants. SHS is characterized by high reaction temperatures (2000−5000 K), fast combustion rates (0.1−200 cm/s), and high temperature gradients (up to 10^6 K/cm). From these properties, other technologically interesting characteristics follow, such as simplicity of the experimental apparatus, intrinsic ability of self-purification, and rapidity of the synthesis. With respect to the latter, SHS reactions are complete in seconds or minutes while conventional methods require hours or days. With SHS, it is also possible to produce materials that are difficult to obtain by other synthetic methods and to achieve chemical synthesis, doping, densification, and shaping in one step. The method has been employed to produce many kinds of materials, such as borides, nitrides, carbides, and hydrides (sometimes also oxides) of transition elements, various intermetallic compounds, and many composite materials (including functionally graded materials).[1−3]

Despite the large amount of published work on the synthesis and characterization of many important materials, little is known about the *chemical* mechanisms of these interesting processes. In fact, the clear technological advantages have encouraged many empirical studies, whereas the mechanistic aspects have received little attention. Some obvious macroscopic similarities have suggested an interpretative approach derived from gas-phase combustion reactions. With this approach, the mechanistic aspects related to the solid nature of reactants and products and to the heterogeneity of the reaction have been frequently neglected relative to aspects of heat production, transmission, and dissipation.

The intrinsic difficulties in understanding the mechanistic aspects of these reactions are also due to experimental reasons (for a recent review on experimental methods used to help understand SHS reactions, the reader is referred to Varma et al.[4]). The study is usually based on analysis of the products at the end of the reaction or after quenching. Shape and speed of the combustion wave can be monitored by video recording. Recently, specific pyrometric methods have been developed,[5] while other methods such as time-resolved X-ray diffraction[6,7] are difficult to use in routine work.

Heat production and dissipation play a central role in this kind of reaction. This is an important difference from most of the traditional chemical kinetics. The importance of the kinetics of energy transport is also shown by the fact that the first theoretical approach to the SHS method is entirely based on these aspects (Merzhanov et al.[8]). In their approach, these authors used Fourier's analysis of heat transfer with a heat source

$$\rho C_p \frac{\partial T}{\partial t} = \chi \frac{\partial^2 T}{\partial x^2} + Q\rho\Phi(T,\eta) \tag{1}$$

$$\Phi(T,\eta) = \frac{\partial \eta}{\partial t} \tag{2}$$

where T is the temperature, η is the degree of conversion, C_p is the heat capacity of the products, ρ is the density, χ is the thermal conductivity, t is the time, x is the spatial coordinate, Q is the thermal effect of the reaction, and Φ is the reaction rate.

An analytical solution of the problem[8,9] has been obtained assuming the kinetic law

$$\frac{\partial \eta}{\partial t} = K_0 \exp\left(-\frac{E_a}{RT}\right)(1-\eta)^n \tag{3}$$

where E_a is an activation energy, K_0 is a preexponential term, and n is the reaction order. Finally, Khaikin and Merzhanov[10]

[†] Department of Physical Chemistry, INCM, and C.S.T.E./CNR, University of Pavia.
[‡] Department of Structural Mechanics, University of Pavia.
[§] University of California.
[⊗] Abstract published in *Advance ACS Abstracts,* September 1, 1997.

S1089-5647(96)03932-6 CCC: $14.00

derived the following expression for the velocity (u) of the *steady combustion wave*

$$u^2 = f(n)K_0\frac{C_p\chi}{Q}\frac{RT_c^2}{E_a}\exp\left(-\frac{E_a}{RT}\right) \quad (4)$$

where $f(n)$ is a function of the order of the reaction.

Using different dilutions of reagents with inert materials or products, it is possible to experimentally achieve different combustion temperatures (T_c). Then, the experimental determination of the combustion speed at different T_c can be used accordingly to obtain the activation energy of the *rate-determining step* of the process from the slope of a $\ln(u/T_c)$ vs $1/T_c$ plot. This approach is important not only because it provides an analytical solution but also because it makes possible the determination of a kinetic parameter (E_a) from coupled measurements of combustion temperature and wave speed. Insight is gained into the reaction mechanism through comparison of the experimental E_a with the activation energy of assumed mechanisms.

Many aspects of SHS processes have been investigated, and different approaches have been used (see, for instance, refs 11−24), but only in relatively few cases has particular attention been given to the experimental investigation of the reaction mechanism or the description of the chemical processes at the level of a single reacting grain.[7,25−33]

From a chemical point of view, the major criticism of the commonly accepted approach is its oversimplified account of the chemical kinetics. Assuming a single reaction step with a homogeneous-phase kinetic law does not provide a realistic basis for modeling SHS processes and hence for providing a clear understanding. Indeed, these reactions involve heterogeneous reactants, an extremely wide range of temperatures and thermal gradients, and a wide range of chemical potentials. It is reasonable to expect that the nature of the most relevant chemical step changes when these variables change. Possible chemical steps include gas-phase, gas/solid, or gas/liquid reactions. They can be diffusion-driven or interface-driven reactions between condensed phases or phase transformations. As a matter of fact, multistep mechanisms are clearly suggested by experimental results. For example, complex wave shapes with large after-burn effects are frequently observed, and there are indications that the chemical nature and physical properties of the products may be controlled by reaction steps well behind the thermal wave leading front.[1]

Understanding the mechanistic aspects is, in our opinion, the most effective approach to the prediction of feasibly and characteristics of SHS reactions. A simple and flexible method was implemented for combining the heat balance equation with the relevant chemistry. The method is devised to include in some way all the sparse indications coming from experiments, to predict the nature of the combustion process, and to provide temperature profiles allowing comparison of results with experiments. In particular, it can include many kinetic models for describing the different chemical and physical steps, in agreement with the current knowledge about the chemical reactivity in heterogeneous systems. Finally, the method can give insight for further experiments to test the importance and features of each step of the model.

The present paper outlines this approach and discusses results for a fairly simple case of the oxidation of metal particles in pure oxygen gas

$$\mathrm{Zr(solid) + O_2(gas) \rightarrow ZrO_2(solid)} \quad (5)$$

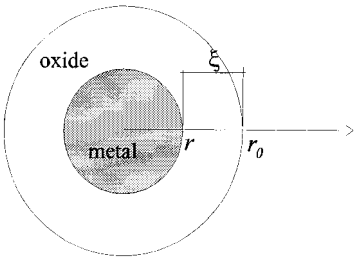

Figure 1. Microkinetic model for the diffusion-controlled oxidation of metal particles in oxygen.

performed in a combustion regime and in the presence of a particular diluent (the reaction product itself).

In future papers this approach will be developed into a model suitable for discussing the thermite reaction

$$\mathrm{Zr + 2NiO \rightarrow 2Ni + ZrO_2} \quad (6)$$

and its predictions will be compared with experimental observations.[34]

2. Computational Method: Oxidation of Metal Particles in a Combustion Regime

2.1. Microkinetic Aspects. Assuming a spherical shape for the metal particles, the oxidation of a single particle is schematically represented by Figure 1. The kinetics can be described by different laws, and the choice of these laws depends on current knowledge about simple mechanisms that control the rate and on particular experimental information. We assume that relevant mechanisms of the oxidation process can be identified with (i) solid-state diffusion of oxygen through the oxide layer and (ii) gas-phase transport of oxygen toward the external surface of the metal particle.

If the kinetics are controlled by solid-state diffusion in the product layer, and with the additional assumptions of isothermal steady-state diffusion and constant molar volume, it is possible to apply the relationship derived by Fromhold[35] that relates to the schematic representation of Figure 1:

$$\frac{d\xi}{dt} = \frac{\Omega}{\left[1 - \left(\frac{\xi}{r_0}\right)\right]\xi} \quad (7)$$

where $\xi \equiv r_0 - r$, r is the radius of the unoxidized particle, r_0 is its initial radius, and Ω is the *tarnishing* constant, which is a function of temperature and, possibly, of oxygen partial pressure. It is expressed as

$$\Omega = \Omega_0 \exp(-E_a/RT) \quad (8)$$

where Ω_0 is a constant, E_a is the activation energy for the process, T is temperature, and R is the gas constant.

We stress here that less restrictive hypotheses can be considered when necessary. For instance, a Dünwald−Wagner[36] power series expansion can be used if one does not want to assume a steady-state diffusion. Also, a more accurate treatment ideally takes into account the coupling between mass and heat transport.

A second mechanism to consider is the assumption that the metal particles are embedded in a uniform atmosphere of oxygen gas and that the oxidation kinetics are controlled by the arrival of oxygen molecules to the external surface of the reacting particle. The kinetics of oxide layer growth will then be given by

$$\frac{d\xi}{dt} = \frac{J_g M_{ox}}{\rho_{ox}}\left(\frac{r_0}{r_0 - \xi}\right)^2 \quad (9)$$

where J_g is the flux of oxygen molecules sticking on the surface of the metal, M_{ox} is the molecular weight of the oxide, ρ_{ox} is its density, and r_0 and ξ are as defined in eq 7. The oxygen flux depends on temperature and pressure as described by the kinetic theory of gases

$$J_g = f\frac{P}{A\sqrt{(2\pi mkT)}} \quad (10)$$

where f is an appropriate sticking coefficient ($0 < f \leq 1$), m is the mass of the oxygen molecule, A is the area, and the other symbols have their usual meaning.

Taking into account two mechanisms (two microkinetic laws) simply means that solid-state diffusion is rate determining under high oxygen partial pressures, the molecular flux toward the particle surface is rate determining under sufficiently low oxygen partial pressures, and other competitive processes are neglected. To find which mechanism is rate determining, we simply compare the gas-phase oxygen flux (J_g, eq 10) with the solid-state diffusion flux (J_{diff}):

$$J_{diff} = \frac{\rho_{ox}}{M_{ox}}\left(\frac{r_0 - \xi}{r_0}\right)\frac{\Omega}{\xi} \quad (11)$$

When $J_g < J_{diff}$, the kinetics are controlled by gas-phase transport; otherwise, it is controlled by solid-state diffusion.

Now, *for a single zirconium particle* and for reaction 6 we can define a conversion degree as

$$\eta = \frac{r_0^3 - (r_0 - \xi)^3}{r_0^3} \quad (12)$$

or, in differential form, as

$$\frac{d\eta}{dt} = \frac{3(1-\eta)^{2/3}}{r_0}\frac{d\xi}{dt} \quad (13)$$

where $d\xi/dt$ is either given by eq 7 or by eq 9, depending on the rate-controlling mechanism in the oxidation process, as indicated above.

2.2. Macrokinetic Aspects. Up to now, the discussion has concerned a single reacting particle, a case we can refer to as the microkinetic aspect. To discuss the combustion process of the whole sample (the macrokinetic aspect), we replace the microkinetic variables (thickness of diffusion layers, particle temperature, oxygen activity in the surrounding pores, etc.) with corresponding macrokinetic variables. These are assumed to be *continuous* variables of time and position within the sample. In particular, for the amount of each chemical component in each phase, we can *define* a set of variables (which we tentatively refer to as *concentrations*) to indicate the corresponding molar quantities per unit volume. Generally, these variables are related to each other by the stoichiometry of the various reaction steps (which also describes the corresponding heat balance).

In the present preliminary example, a single reaction step 5 is considered and only two *concentrations* are required. We denote with a and b the molar amount (per unit volume) of metal and metal oxide in their pure solid phases. As a further simplification, we assume that all metal particles have the same size and that metal and diluent particles are uniformly packed in the starting sample. Then, the starting a and b values (a_0 and b_0) are experiment-specific numbers.

Now, the a and b "concentrations" are related to each other by the stoichiometry of the reaction step 5, so that a more convenient variable is the macrokinetic degree of conversion (a function of space and time). This parameter can be described as

$$\eta = \frac{a_0 - a}{a_0} \quad (14)$$

and is identified with the microkinetic η.

For further simplicity, we consider a sample in the shape of a cylinder, surrounded by a constant and uniform oxygen atmosphere, and we work out a one-dimensional model (i.e. neglecting temperature and compositional variations along the radial coordinate of the sample and oxygen permeation through the heterogeneous sample). Finally, space and time evolution of the macrokinetic variables T and η obey the macrokinetic laws (1 and 2), where

$$Q\Phi(T,\eta) = -a_0\Delta H_{ox}(T)\frac{\partial\eta}{\partial t} \quad (15)$$

$$\frac{\partial Q_{ox}}{\partial t} = -\frac{\partial b}{\partial t}\Delta H_{ox}(T) = -a_0\Delta H_{ox}(T)\frac{\partial\eta}{\partial t}$$

and

$$\left.\frac{\partial\eta}{\partial t}\right|_{diff} = \frac{3\Omega(1-\eta)^{1/3}}{r_0^2[1-(1-\eta)^{1/3}]} \quad (16)$$

$$\left.\frac{\partial\eta}{\partial t}\right|_{g} = \frac{3J_g M_{ox}}{r_0\rho_{ox}} \quad (17)$$

(M_{ox} and ρ_{ox} are the molar weight and the density of the oxide product).

The main point of the present method is therefore to identify, for each step of the SHS process, the macrokinetic temperature with the temperature of the microkinetic law (see eq 7, where Ω depends on temperature) and to identify the macrokinetic variable η with the microkinetic η, i.e. to use eq 13 to describe the time evolution of the space and time variable defined by eq 14.

In the present approach the heterogeneous system is then described at the macrokinetic level as a homogeneous system, an approximation justified by the fact that the specific aspects of each heterogeneous reaction are already taken into account by the microkinetic laws. Assumptions regarding the sample microstructure are required but do not represent strong limitations on the characteristics that can be investigated by this approach. For instance, it is possible to study an SHS process where reactant and diluent particles are mixed in different proportions along the sample, a case important in modeling the synthesis of *functionally graded materials* (FGM). Particular features of an SHS process are generally enclosed in the initial conditions of the continuous composition variables. It is also possible to treat long-range diffusion processes that are different from true solid-state diffusion at the macrokinetic level. The permeation of a gaseous reactant from the outer surface of the sample pellet or the diffusional spread of a gaseous intermediate product are examples. Inserting the relevant Fick's laws into the set of macrokinetic equations can do this.

Other quantities are required to work out a numerical solution. Briefly, the phase densities are related by

$$\frac{aM_{\mathrm{M}}}{\rho_{\mathrm{M}}} + \frac{bM_{\mathrm{ox}}}{\rho_{\mathrm{ox}}} + \frac{c_0 M_{\mathrm{dil}}}{\rho_{\mathrm{dil}}} + p = 1 \tag{18}$$

where M_{M}, M_{ox}, and M_{dil} are the molecular weights of the metal, oxide, and diluent, respectively, ρ_{M}, ρ_{ox}, and ρ_{dil} are the corresponding densities, p is the relative porosity, and c_0, analogous to a and b, is the "concentration" of a diluent phase other than the reaction product.

Global heat capacities and thermal conductivities are defined as

$$\bar{C}_p = aC_{p,\mathrm{M}} + bC_{p,\mathrm{ox}} + c_0 C_{p,\mathrm{dil}} \tag{19}$$

$$\chi = \frac{aM_{\mathrm{M}}}{\rho_{\mathrm{M}}}\chi_{\mathrm{M}} + \frac{bM_{\mathrm{ox}}}{\rho_{\mathrm{ox}}}\chi_{\mathrm{ox}} + \frac{c_0 M_{\mathrm{dil}}}{\rho_{\mathrm{dil}}}\chi_{\mathrm{dil}} \tag{20}$$

The very approximate nature of eq 20 should be noted: other phenomenological models may be required, for instance, and we may refer to the percolative model developed[21] for electrical conductivity.

2.3. Numerical Aspects. The basic equations of the model without a foreign diluent are

$$a = a(x,t) = a_0(1-\eta) \tag{21}$$

$$b = b(x,t) = b_0 + a_0\eta$$

$$\bar{C}_p = aC_{p,\mathrm{M}} + bC_{p,\mathrm{ox}} \tag{22}$$

$$\chi = \frac{aM_{\mathrm{M}}}{\chi_{\mathrm{M}}}\chi_{\mathrm{M}} + \frac{bM_{\mathrm{ox}}}{\chi_{\mathrm{ox}}}\chi_{\mathrm{ox}} \tag{23}$$

$$\frac{\partial\eta}{\partial t}\Big|_{\mathrm{diff}} = \frac{3\Omega_0 \exp(-E_a/RT)(1-\eta)^{1/3}}{r_0{}^2[1-(1-\eta)^{1/3}]} \tag{24}$$

$$\frac{\partial\eta}{\partial t}\Big|_{\mathrm{g}} = \frac{3J_{\mathrm{g}}M_{\mathrm{ox}}}{r_0\rho_{\mathrm{ox}}} \tag{25}$$

$$\frac{\partial\eta}{\partial t} = \min\left[\frac{\partial\eta}{\partial t}\Big|_{\mathrm{diff}}, \frac{\partial\eta}{\partial t}\Big|_{\mathrm{g}}\right] \qquad 0 \le \eta \le 1 \tag{26}$$

$$\bar{C}_p\frac{\partial T}{\partial t} = \frac{\partial}{\partial x}\left(\chi\frac{\partial T}{\partial x}\right) - a_0\Delta H_{\mathrm{ox}}(T)\frac{\partial\eta}{\partial t} - \frac{2\sigma\epsilon}{R_{\mathrm{c}}}(T^4 - T_0{}^4) \tag{27}$$

where σ is the Stefan−Boltzmann constant, ϵ is the emissivity, R_{c} is the radius of the sample, T is the temperature, T_o is the initial (ambient) temperature, and the other symbols are defined previously.

The initial and boundary conditions are

$$t = 0, \quad 0 \le x \le x_{\mathrm{s}} \qquad \begin{cases} T = T_{\mathrm{s}} \\ \eta = 1 \end{cases}$$

$$t = 0, \quad x_{\mathrm{s}} \le x \le \infty \qquad \begin{cases} T = T_0 \\ \eta = 0 \end{cases}$$

$$t = 0, \quad x = 0 \qquad \begin{cases} T = T_{\mathrm{s}} \\ \eta = 0 \end{cases}$$

$$t > 0, \quad x \to \infty \qquad \begin{cases} T = T_0 \\ \eta = 1 \end{cases} \tag{28}$$

where T_{s} and x_{s} are two parameters that can be varied at will in large ranges (T_{s} must be close to, or higher than, the adiabatic temperature). As a matter of fact, the values have an influence (to a small extent) only on the nonstationary part of the numerical results. The simplicity of the boundary and initial condition will be later modified to discuss the SHS startup in more detail.

In the most general case of an SHS process with n steps, the entire partial differential equation (PDE) system can be written as

$$\frac{\partial T}{\partial t} = \alpha\frac{\partial^2 T}{\partial x^2} + \beta\frac{\partial T}{\partial x} + \gamma$$

$$\frac{\partial\eta_i}{\partial t} = f(\eta_i, T); \quad i = 1, ..., n \tag{29}$$

which shows that it is a parabolic PDE system. In particular, α is a term containing the thermal conductivity, β is a term containing the gradient of thermal conductivity, and γ is the forcing term of the energy balance equation and describes heat production and dissipation, i.e.

$$\alpha = \frac{k}{\bar{C}_p}; \quad \beta = \frac{1}{\bar{C}_p}\frac{\partial k}{\partial x} \tag{30}$$

$$\gamma = \sum_i\left(\frac{Q}{\bar{C}_p}\frac{\partial\eta_i}{\partial t}\right) - \frac{2\sigma\epsilon}{\bar{C}_p R_{\mathrm{c}}}(T^4 - T_0{}^4)$$

The numerical solution of this system has been obtained with finite difference methods. After a few trials with different algorithms, we finally adopted the Crank−Nicholson scheme,[37] which is accurate to the second order in the truncation error and is unconditionally stable. Lower-upper triangular (LU) decomposition with forward and backward substitution has been used to solve the resulting tridiagonal set of algebraic equations. The chemical equations $\partial\eta/\partial t = f(\eta,T)$ have been integrated using (a) for $\partial\eta/\partial t|_g$, a Euler algorithm; (b) for $\partial\eta/\partial t|_d$, a fourth-order Runge−Kutta algorithm[38] or (with similar performance) a Brent algorithm[38] based on the implicit form of the analytic solution.

The basic assumption that the SHS process considered here can be described by a single step requires that the phase transitions for both Zr metal and zirconia be neglected. For this reason, a set of suitably modified thermodynamic data has been employed. These modified data have been chosen as follows. First of all, the reaction enthalpy of the reaction has been described by

$$\Delta H/\mathrm{J\ mol^{-1}} = 1\,099\,179 + 10.366T \tag{31}$$

as obtained by a single linear best fit of the whole set of experimental data (i.e. including the effect of phase transitions of reactant and product). Then, the heat capacity of zirconia up to 2112 K has been described by

$$C_p(\mathrm{ZrO_2})/\mathrm{J\ mol^{-1}\ K^{-1}} = a + b(T) + c(T)^2 + d(T)^{-2} \qquad (T > 2112\ \mathrm{K}) \tag{32}$$

$$a = 72.79; \quad b = 5.53 \times 10^{-3}; \quad c = -1.39 \times 10^{-6}; \quad d = -16.95 \times 10^5$$

and has been analogously obtained by a best fit of the known heat capacities of monoclinic, tetragonal, and cubic zirconia (again treated as a single set of data). Above 2112 K, the heat capacity is kept constant at the maximum value given by this

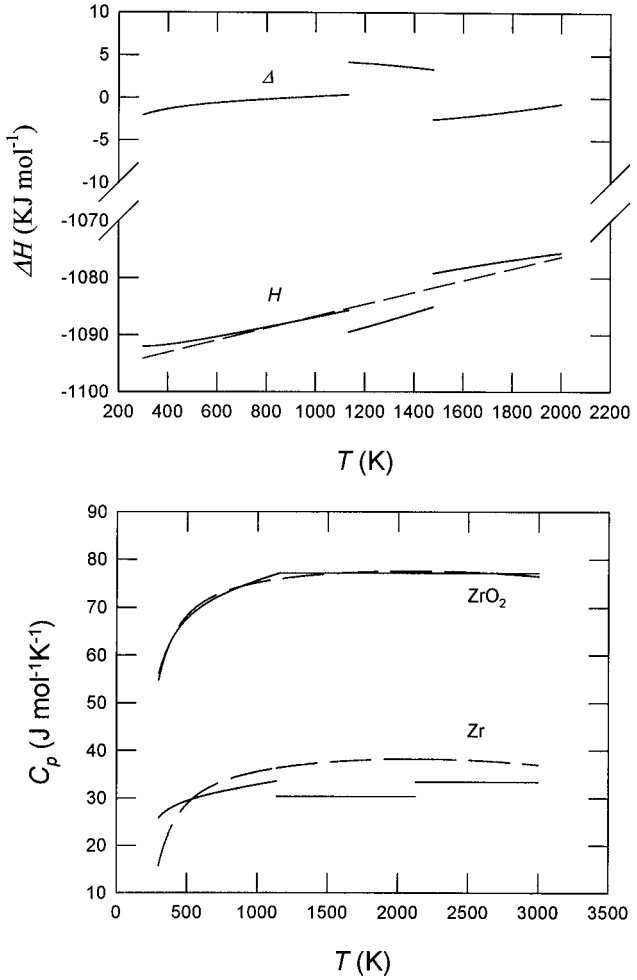

Figure 2. Thermodynamic data for the oxidation of zirconium. The lower plot shows the molar heat capacities of Zr and ZrO_2 used in the present approach (continuous lines) compared with the experimental data (dashed lines, the breaks correspond to phase transitions). The upper plot analogously shows the reaction enthalpy (H) data: Δ marks the enlarged difference between solid and dashed curves.

expression. The heat capacity of gaseous oxygen has been taken as

$$C_p(O_2) = 29.16 \text{ J mol}^{-1} \text{ K}^{-1} \quad (33)$$

(i.e. as temperature independent). Finally, for thermodynamic consistency, the heat capacity of Zr has been back-calculated from the above expressions for $C_p(O_2)$, $C_p(ZrO_2)$, and ΔH:

$$C_p(Zr) = C_p(ZrO_2) - C_p(O_2) - d\Delta H/dT = a' + b(T) + c(T)^2 + d(T)^{-2} \quad (34)$$

Figure 2 compares the thermodynamic functions used in this work with the corresponding true values.

For the tarnishing constant Ω (see eq 8) we used[39]

$$\Omega_0 = 0.4361 \times 10^{-5} \text{ m}^2 \text{ s}^{-1} \quad (35)$$

$$E_a = 176.5 \text{ kJ mol}^{-1}$$

In agreement with the current knowledge about the vacancy mechanism of oxygen diffusion in solid zirconia and defect equilibria in this material, the tarnishing constant is assumed to be independent of oxygen pressure.

The emissivity of the sample has been arbitrarily set to 0.4. For the thermal conductivities, we have used the temperature-independent values

$$\kappa(Zr) = 35.5 \text{ W m}^{-1} \text{ K}^{-1} \quad (36)$$

$$\kappa(ZrO_2) = 4.15 \text{ W m}^{-1} \text{ K}^{-1}$$

as typical values for a metal and a ceramic material.

The sample radius, R_c, has been set at 0.01 m. The density of Zr and zirconia were taken as 6494 and 5600 kg m^{-3}, independent of temperature.

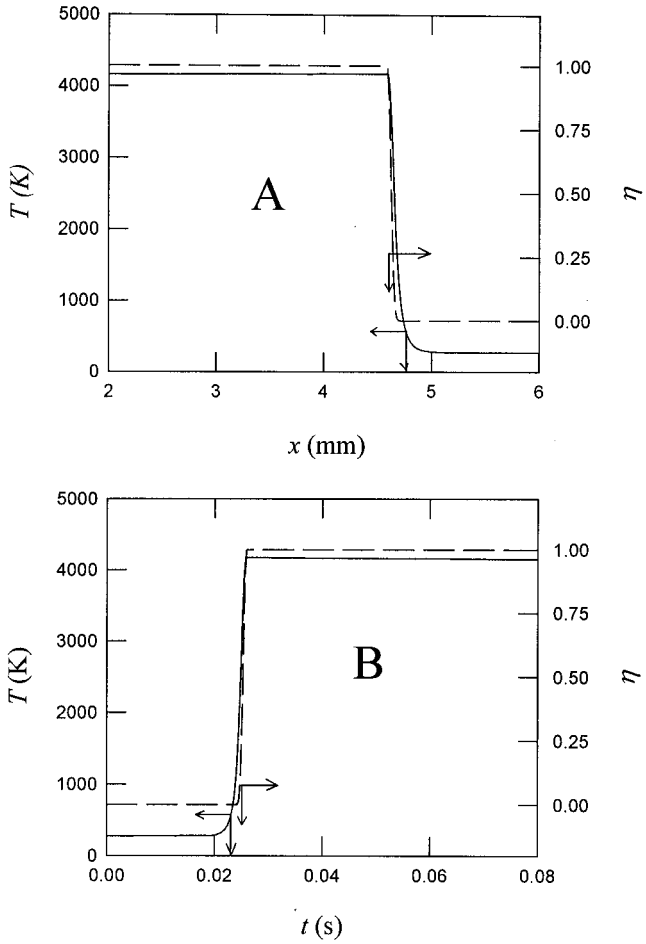

Figure 3. Oxidation under 1 atm oxygen partial pressure of a sample of monosized (r_0 = 10 μm) Zr particles diluted with 75% (by mole) zirconia. Temperature (continuous lines) and composition (dashed lines) profiles as a function of position within sample at fixed time (A) or as a function of time at fixed position within sample (B).

3. Results and Discussion

Consider the oxidation of a sample of monosized (r_0 = 10 μm) zirconium particles diluted with 75% (by mole) of zirconia powders and surrounded by a uniform environment of gaseous oxygen at 1 atm pressure. The shapes of the temperature $T = T(x,T)$ and composition $\eta = \eta(x,T)$ profiles are shown either (upper plot of Figure 3) as $f(x)$ at fixed t (x = position within the sample, t = reaction time) or as $f(t)$ at fixed x (lower plot of Figure 3). The η profiles (dashed lines) are steeper than the T profiles (continuous lines), an observation consistent with the understanding that the initiation of the chemical reaction requires preheating. The shape of the chemical wave is better appreciated by its time derivative, as illustrated by Figure 4 (hereafter, the partial derivative $(\partial\eta/\partial t)_x$ will be referred to as the reaction rate).

In the simple SHS model discussed here, there are three process parameters: size of the reactant zirconium particles (r_0),

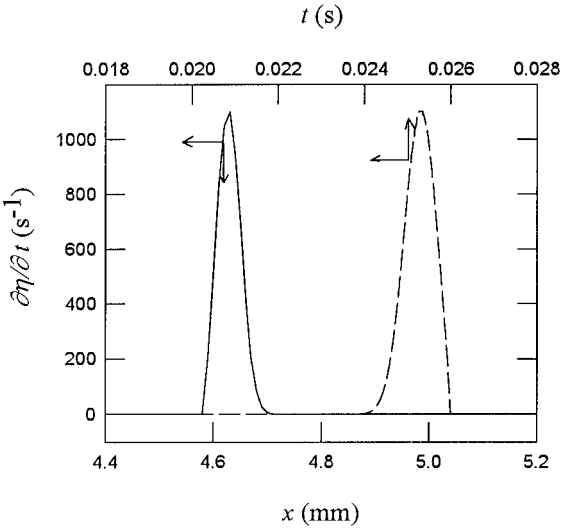

Figure 4. Rate of the chemical reaction as a function of position within sample at fixed time (continuous line) and as a function of time at fixed position (dashed line) for the case of the previous figure.

dilution degree, and oxygen partial pressure. Our method gives a simple and direct tool for exploring the effect of each parameter on the feasibility, features, and predominant mechanism of the SHS process.

We consider first the effect of oxygen pressure, $P(O_2)$. Plot C of Figure 5 shows the thermal profiles at a fixed time for $P(O_2)$ ranging from 0.01 to 1 bar. The other parts of the same figure show the corresponding profiles of the reaction rate ($\partial\eta/\partial t$). The profiles change from bell-shaped (A) to more complex shapes (B, D, and E). These changes mark the transition from a reaction entirely controlled by solid-state diffusion to a situation where the chemical reaction starts under diffusion control, proceeds under gas pressure control, and is again under diffusion control at the end. The change of mechanism is well illustrated by Figure 6, where the dotted lines show the reaction rates according to the single mechanisms (diffusion or gas pressure control), while the continuous line shows the overall rate and the dashed line shows the temperature. One can clearly see (i) the onset of diffusional growth due to the temperature rise, (ii) the effect of external oxygen cutting the bell-shaped diffusional curve, and (iii) the final stage where the lower conversion rate is essentially due to the effect on diffusion of the finite dimension of the reacting particle. From a macrokinetic point of view, one might foresee a transition from a pressure-dependent regime, where the wave speed is heavily affected by the external pressure, to a pressure-independent regime where the reaction rate is under diffusion control over the entire reaction front. This inference is well supported by the numerical results (parts a and b of Figure 7). As already stated, in our model the latter mechanism does not depend on external oxygen pressure.

The effect of particle size is shown in Figure 8 for a fixed oxygen pressure (0.032 bar). Plot C shows the effect on the thermal wave. With this external pressure, gas-phase transport plays a significant role in the case of smaller-sized particles (plots A, B, and D), whereas solid-state diffusion is the predominant effect in the case of larger particles (plot E).

For higher external pressures, the region where diffusion predominates extends to smaller sizes. Particle size affects the macrokinetics of the SHS in a simple way: a proportional dependence of wave speed on the inverse particle size has been empirically found in some previous experiments.[40,41] Despite the simple nature of the present model, it shows quite clearly (Figure 9) an inverse relationship at higher pressure, where

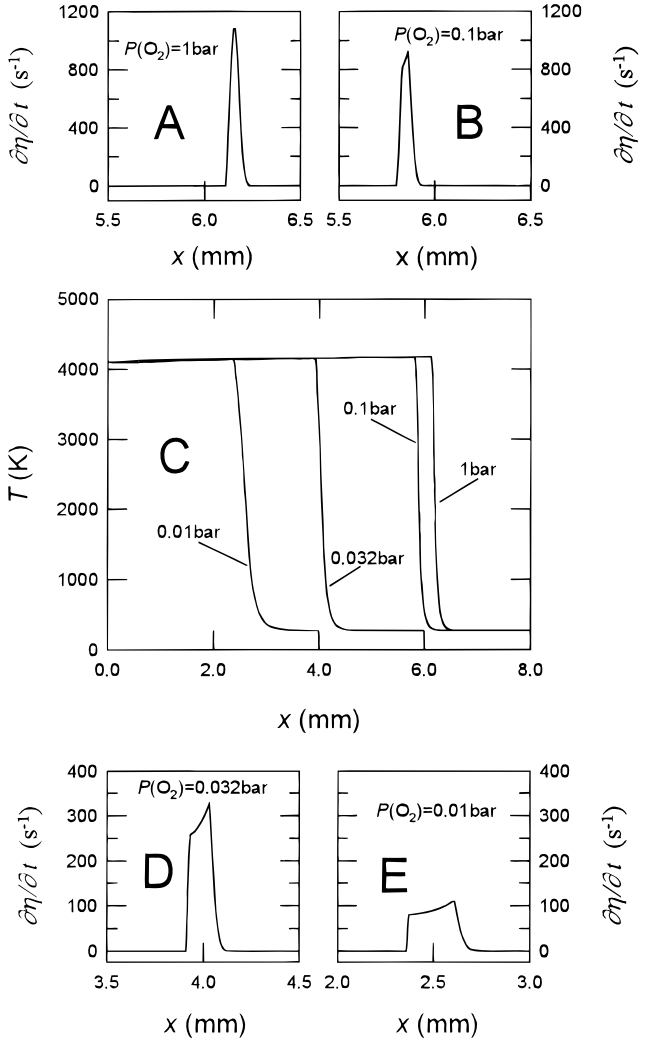

Figure 5. Oxidation under different oxygen partial pressures of a sample of monosized ($r_0 = 10\ \mu$m) Zr particles diluted with 75% (by mole) zirconia. Plot C, thermal waves; plots A, B, D, and E reaction rates.

diffusion control is operative. Such an inverse relationship is not valid under conditions of pressure-dependent kinetics.

The effect of dilution was also investigated. Figure 10 shows that diluting the reacting mixture has a similar effect on the mechanism as raising the oxygen pressure or increasing the particle size (plots A, B, D, and E). A new feature arises here, because the combustion wave is no longer stationary when a high dilution level is used (plot C: curve for 85% by mole of zirconia in the starting mixture). Unsteady propagation can be directly seen in the irregular trends of the thermal and chemical waves (Figure 11, plots A and B) or in the oscillatory behavior of reaction rates and wave speeds (Figure 11C,D) but is more easily appreciated by plotting against each other the (temperature, wave speed) values corresponding to the peak of each rate profile at different reaction times (Figure 12). In these diagrams, the curves describing the time evolution of the process (i) begin from a point that depends on the (T_s, x_s) parameters used to start up the SHS and (ii) eventually approach a stationary point or a limiting cycle, which depends on run parameters but does not depend on the (T_s, x_s) parameters.

While a reliable approach to the chemical aspects of features such as nonstationary propagation, oscillations, and instabilities requires a 3D model, this figure can be taken as a preliminary indication that the method can indeed explore in some ways more complex features of SHS.

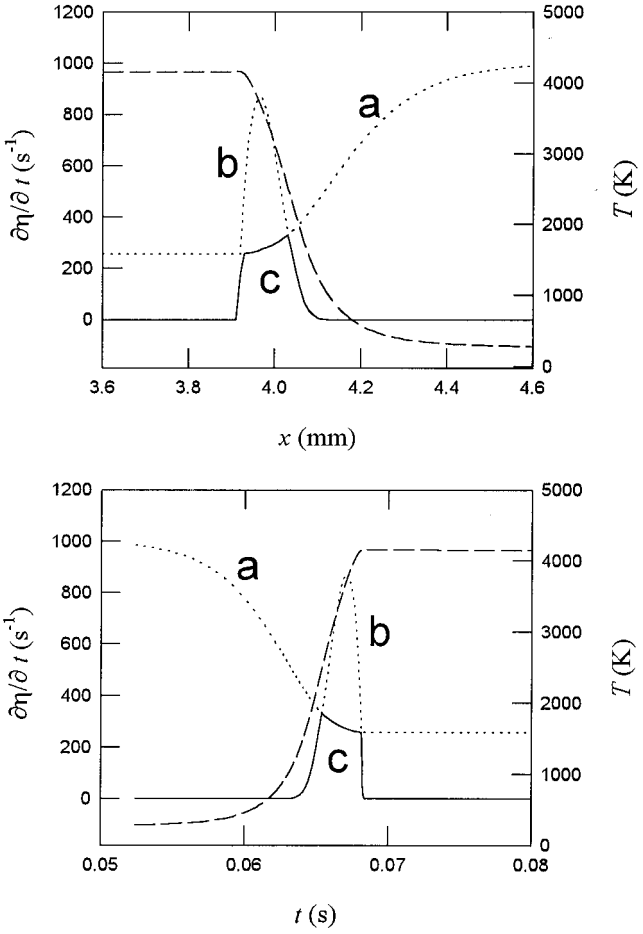

Figure 6. Sticking rate of gaseous oxygen (a, dotted line), diffusional growth (b, dotted line), overall reaction rate (c, continuous line), and particle temperature (dashed line) for the oxidation of a sample of monosized (r_0 = 10 μm) Zr particles diluted with 75% (by mole) zirconia, under $P(O_2)$ = 0.032 bar.

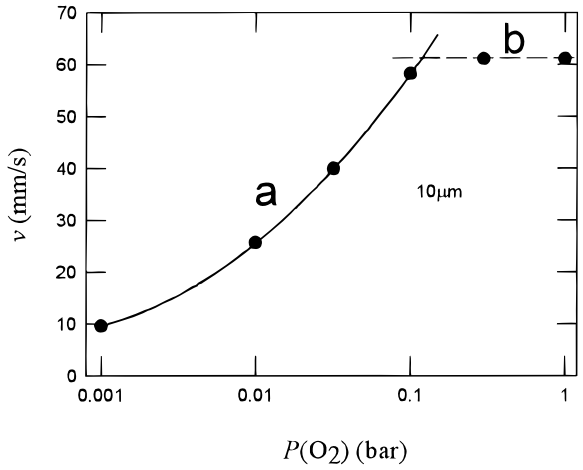

Figure 7. Wave speed under different oxygen partial pressures for the oxidation of a sample of monosized (r = 10 μm) Zr particles diluted with 75% (by mole) zirconia. Part a of the plot corresponds to a pressure-dependent regime and part b to pressure independent, diffusion-controlled kinetics.

Finally, we note that the last set of experiments corresponds to what is actually required to use a $\ln(u/T_c)$ vs $1/T_c$ plot of Merzhanov's analysis[10] (see eq 4). It is therefore interesting to compare the outcome of the present approach with the predictions of this theory. The comparison is shown on Figure 13. T_c is the maximum of the thermal wave, filled squares and open circles respectively refer to 1 and 0.032 bar oxygen pressure, labels a, ..., e indicate different dilutions, and the error bars on the lower T_c points correspond to the upper and lower values on the limiting cycles of the (T, rate) diagrams (Figure 12). The highest T_c data are pressure dependent because of the onset of gas-phase control at the lower oxygen pressure. The

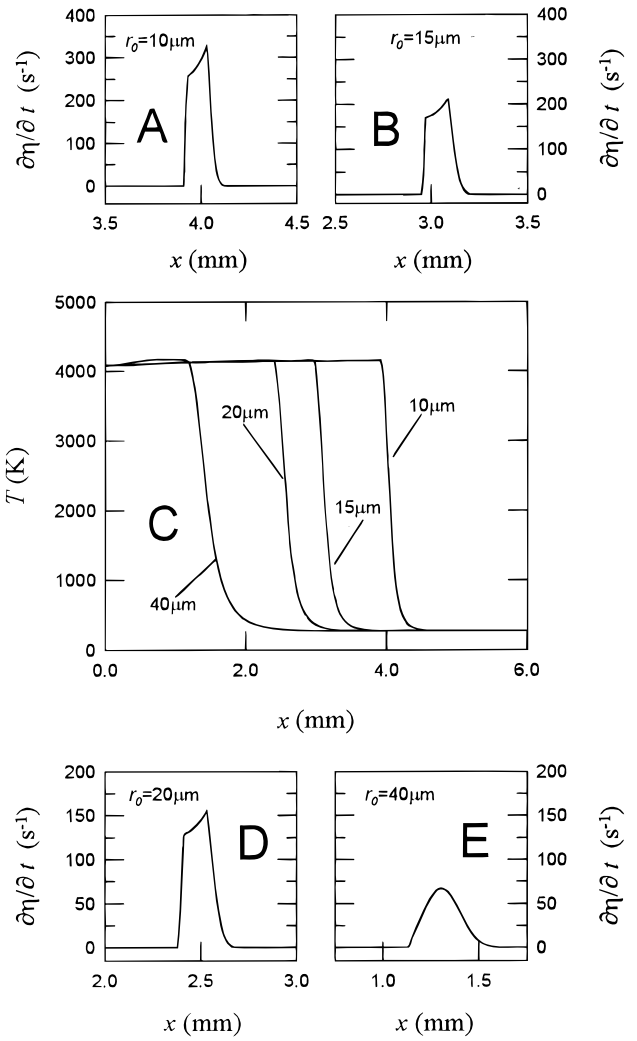

Figure 8. Oxidation under 1 atm oxygen partial pressure of a sample of monosized Zr particles with different sizes and diluted with 75% (by mole) zirconia. Plot C, thermal waves; plots A, B, D, and E, reaction rates.

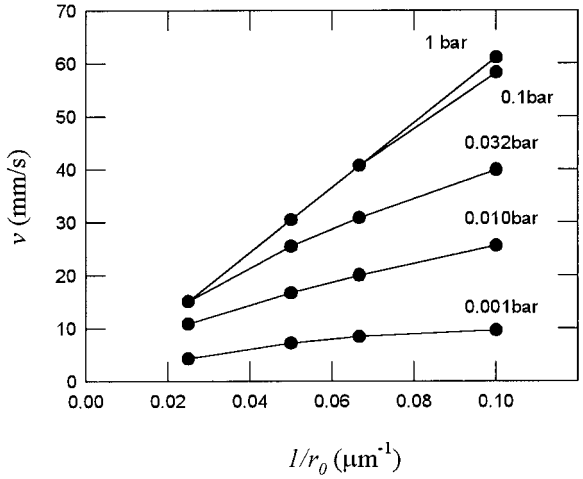

Figure 9. Wave speed for the oxidation of differently sized Zr particles diluted with 75% (by mole) zirconia; the continuous lines connect data under the same oxygen partial pressure.

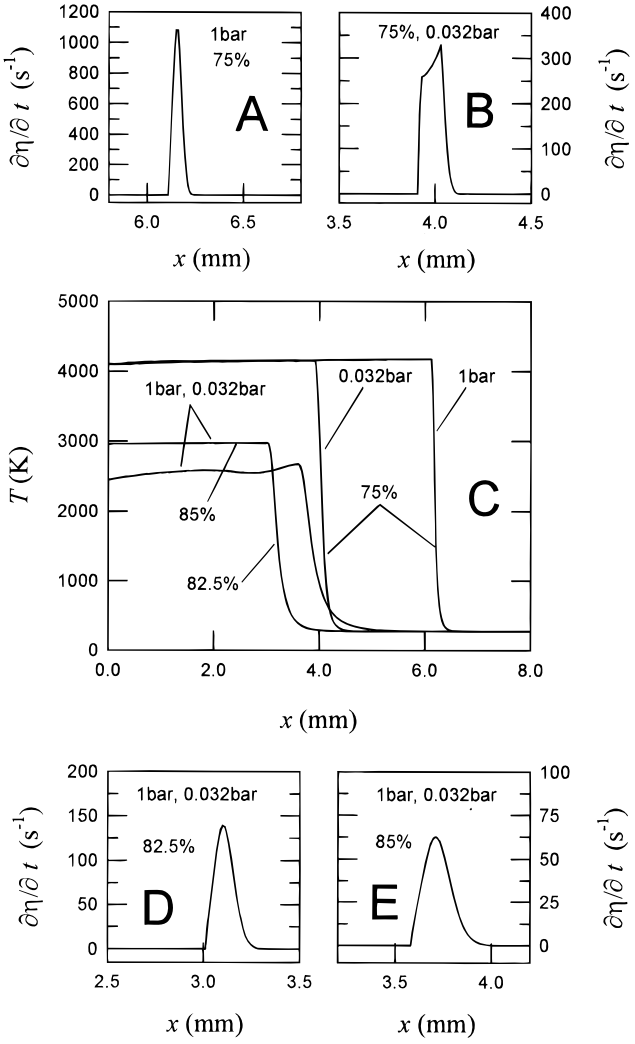

Figure 10. Oxidation under different oxygen partial pressures of a sample of monosized Zr particles ($r_0 = 10\ \mu$m) diluted with different amounts of zirconia: C, thermal waves; A, B, D, E, reaction rates. The thermal wave (C) for 85% dilution and 1 bar oxygen pressure shows the onset of oscillatory behavior.

change of mechanism is clearly shown by a drift of the low-pressure data (filled squares) from linear behavior: a regression line through the filled squares gives $E_a = 120$ kJ mol^{-1}, which is 32% lower than the real activation energy of oxygen diffusion in zirconia (176.5 kJ mol^{-1}). The regression line through the open circles gives a much closer value (153 kJ mol^{-1}).

4. Summary

The paper presents a very simple application of a general method for investigating the *chemical aspects* of SHS processes. The guidelines of the method can be summarized as follows:

An SHS reaction is divided into several (n) steps. A step can be a chemical reaction or a phase transformation. The various steps are coupled to each other by mass and energy balance constraints, as summarized by the corresponding stoichiometric equations.

A reaction step, in turn, is described by one or more kinetic laws (by one or more mechanisms). Candidate mechanisms for a particular step are suggested by analogy with other similar processes and by the analysis of experimental results.

By mechanism we mean a microkinetic law, i.e., a phenomenological equation that describes the reaction step at the scale of the grains of the reactant phases. Many simplifying assumptions are made here, about microstructure (size, shape, distribution of the grains) and dependence on external conditions. For instance, we may assume at this stage some steady state approximation to the solution of Fick's equations, or we may neglect the coupling of matter and energy fluxes. Also, the microkinetic laws are typically (but not necessarily) derived under the assumption of isothermal conditions.

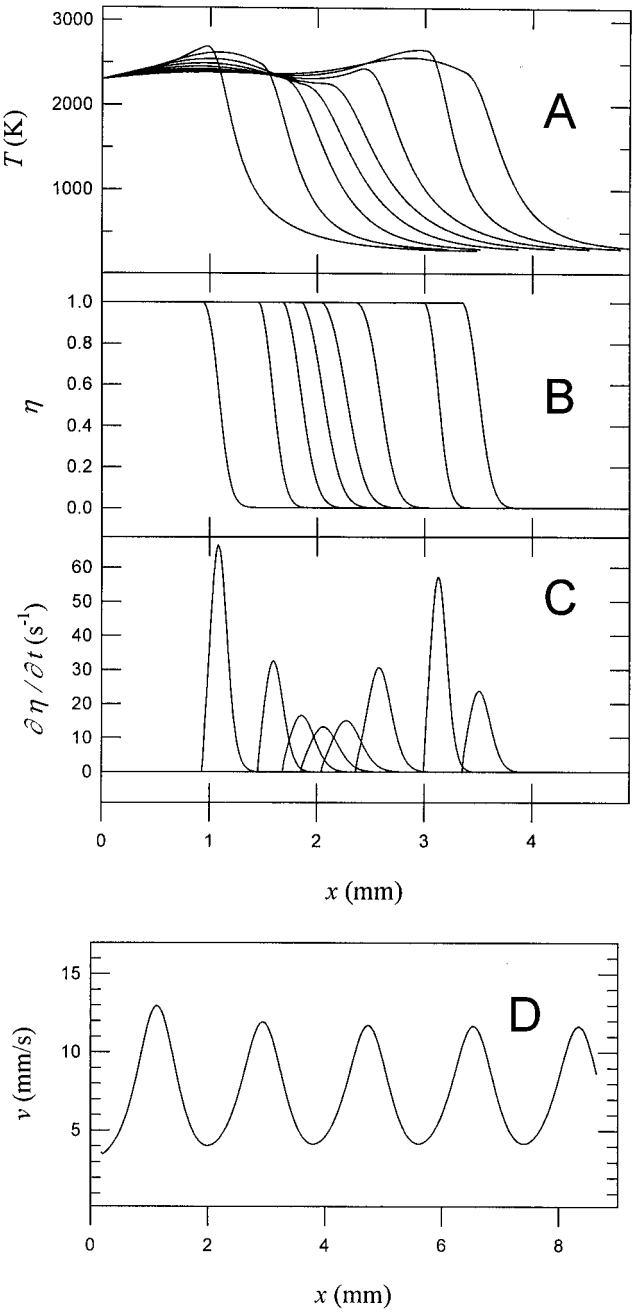

Figure 11. Oxidation under 1 bar oxygen partial pressures of a sample of monosized Zr particles ($r_0 = 10\ \mu$m) diluted with 86% (by mole) of zirconia. Plot A, thermal wave; plot B, chemical wave; plot C, reaction rate; plot D, wave speed. The T, η, and $\partial\eta/\partial t$ profiles are shown at 0.05 s intervals.

For each reaction step, a single kinetic law holds for a given set of external (local) conditions, i.e., the mechanism corresponding to the slowest rate.

The various microkinetic parameters (diffusion layers, temperature, component activities, etc.) typical of each mechanism are then replaced by a set of appropriate macrokinetic variables that are explicitly written as functions of space and time.

The space and time dependence of the independent macrokinetic variables (degree of conversion η_i and temperature T)

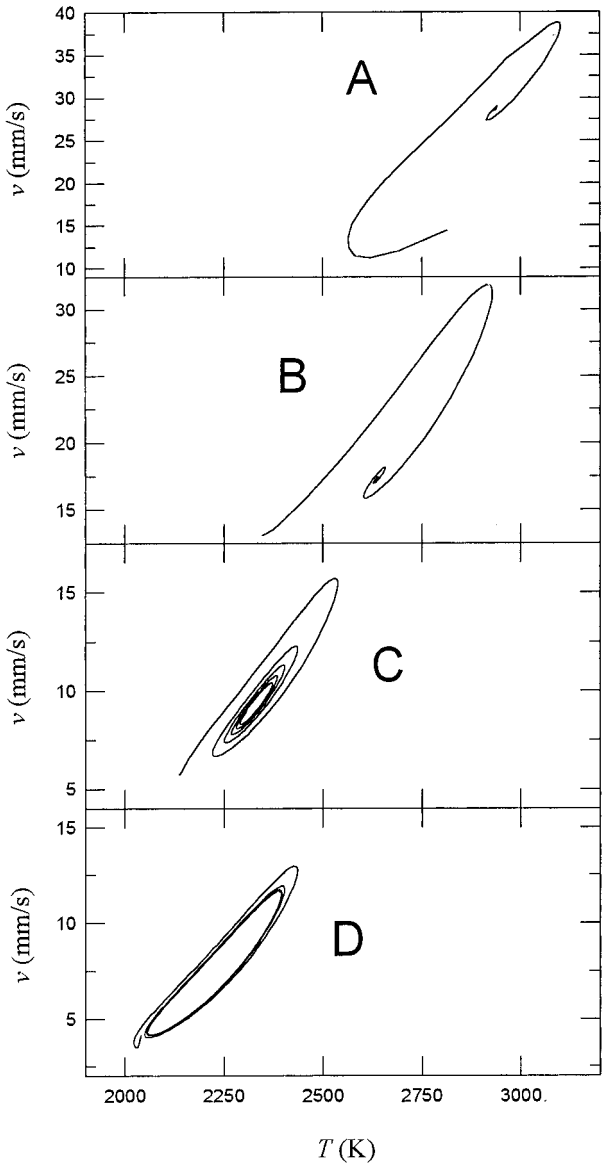

Figure 12. Time evolution of the wave speed (v) and the temperature at maximum rate (T) and for the oxidation under 1 bar oxygen partial pressure of a sample of monosized ($r_0 = 10$ μm) Zr particles diluted with different amounts of zirconia. Plot A, 86%; plot B, 85%; plot C, 82.5%; plot D, 80% of diluent by mole.

are obtained by solving the $n + 1$ equations

$$\frac{\partial \eta_i}{\partial t} = f(\eta_i, T); \quad i = 1, ..., n$$

$$\bar{C}_p \frac{\partial T}{\partial t} = \frac{\partial}{\partial x}\left(\chi \frac{\partial T}{\partial x}\right) + \sum_i \left(Q_i \frac{\partial \eta_i}{\partial t}\right) - \delta \qquad (37)$$

where each macrokinetic equation i comes from the underlying microkinetic law, while δ includes all dissipation terms (by convection and radiation). Possible extension of the present method can include other transport phenomena, such as long-range diffusion, which is expected to play an important role in some gas/solid or gas/liquid reactive steps.

Other parameters required by the macrokinetic equations (thermal conductivity, heat capacity, ...) are analogously written as functions of space and time, using balance constraints and—when necessary—suitable phenomenological models for heterogeneous materials.

The particular example worked out here is clearly oversimplified. For instance, neglecting the filtration of the gaseous

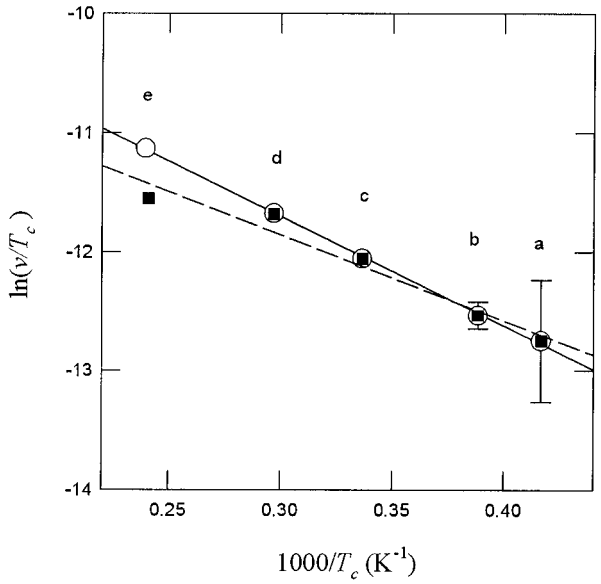

Figure 13. Combustion temperature (T_c) and wave speed (v) for the oxidation under 1 bar (open circles) or 0.032 bar (filled squares) oxygen partial pressure of a sample of monosized ($r_0 = 10$ μm) Zr particles diluted with different amounts of zirconia (a, 75%; b, 80%; c, 82.5%; d, 85%; e, 86% of diluent by mole).

reactant into the porous heterogeneous sample cannot be justified, and we do not claim that the present model provides direct insights into the simple $Zr + O_2$ combustion synthesis. Things are different, however, for thermite reactions 6, where oxygen is supplied by thermal decomposition of another oxide. Therefore, the present results are best viewed, as already said, as a preliminary step toward more complex SHS processes.

The present model is oversimplified also because it does not take into account phase transformations in reactant and product phases. This is, however, a minor limitation: as pointed out in the previous guidelines, our approach can analyze an SHS process using several different steps, which can be phase transformations as well as chemical reactions.

Despite these limitations, however, the present example provides in our opinion many insights into the usefulness of the method. From the point of view of mechanistic studies, the results indicate, for instance, that the shape of the combustion waves (both the thermal and chemical waves) and their speed are sensible tools for gaining information on the nature of the rate-determining step and on its change under different external conditions. As an example, it is very promising that a relationship empirically found between wave speed and particle size has been proven to be related to a reaction mechanism (solid-state diffusion).

Generally, we think that the main power of the present method is its effectiveness as a "what-if" tool. For the reasons given in the Introduction, the mechanisms of SHS processes are very complex and strongly differ from each other even for seemingly related reactions. Then, it is important to have a simple tool for investigating some reasonable candidates for the rate-determining step; in particular, for exploring how the experimentally accessible data (thermal profiles, wave speed) depend on process variables when these mechanisms are taken into account. These numerical simulations can then be compared with experiments both for assessing or discarding some mechanism and for suggesting further experiments. On a whole, this approach is not very different from the trial and error procedure that is usually employed in many experimental investigations on chemical kinetics, and the numerical "experiments" of our simulation procedure take the place of real experiments. The

numerical experiments are especially important because of the scarcity of experimental data. More realistic examples of the effectiveness of this procedure in providing a real understanding of the complexity of SHS reactions will be given in future papers.

Acknowledgment. This work has been partially supported by the Department of University and Scientific and Technological Research of the Italian Government (MURST−40%).

References and Notes

(1) Munir, Z. A.; Anselmi-Tamburini, U. *Mater. Sci. Rep.* **1989**, *3* (7,8) 277.

(2) Holt, J. B.; Dunmead, S. D. *Annu. Rev. Mater. Sci.* **1991**, *21*, 305.

(3) McCauley, J. W. *Ceram. Eng. Sci. Proc.* **1990**, *11* (9−10), 1137.

(4) Varma, A.; Kachelmyer, C. R.; Rogachev, A. S. *Int. J. Self-Propag. High-Temp. Synth.* **1996**, *5* (1), 1.

(5) Anselmi Tamburini, U.; Campari, G.; Spinolo, G.; Lupotto, P. *Rev. Sci. Instrum.* **1995**, *66*, 5006.

(6) Boldyrev, V. V.; Aleksandrov, V. V.; Corchagin, M. A.; Tolochko, B. P.; Gusenko, S. N.; Sokolov, A. S.; Sheromov, M. A.; Lyakhov, N. Z. *Dokl. Akad. Nauk SSSR* **1981**, *259*, 1127.

(7) Rogachev, A. S.; Khomenko, I. O.; Varma, A.; Merzhanov, A. G.; Ponomarev, V. I. *Int. J. Self-Propag. High-Temp. Synth.* **1994**, *3* (3), 239.

(8) Merzhanov, A. G. *Arch. Procesow Spalania* **1974**, *5* (1), 17.

(9) Novikov, N. P.; Borovinskaya, I. P.; Merzhanov, A. G. In *Combustion Processes in Chemical Technology and Metallurgy*; Merzhanov, A. G., Ed.; 1975.

(10) Kaikin, B. I.; Merzhanov, A. G. *Combust., Explos. Shock Waves* **1966**, *2*, 22.

(11) Lakshmikanta, M.; Sekhar, J. A. *J. Am. Ceram. Soc.* **1994**, *77*, 202.

(12) Matkowsky, B. J.; Sivashinsky, G. I. *SIAM J. Appl. Math.* **1978**, *35*, 465.

(13) Margolis, S. B.; Matkowsky, B. J.; Booty, M. R. In *Combustion and Plasma Synthesis of High-Temperature Materials*; Munir, Z. A., Holt, J. B., Eds.; VCH Publishers: New York, 1990; p 73.

(14) Brailovsky, I.; Sivashinsky, G. *Physica D* **1993**, *65*, 191.

(15) Puszynski, J. A.; Kumar, S.; Dimitriou, P.; Hlavacek, V. *Z. Naturforsch.* **1988**, *43A*, 1017.

(16) Subramanian, V.; Lakshnmikantha, M. G.; Sekhar, J. A. *J. Mater. Res.* **1995**, *10*, 1235.

(17) Hlavacek, V.; Dimitriou, P.; Degrève, J.; Scholz, J. In *Combustion and Plasma Synthesis of High-Temperature Materials*; Munir, Z. A., Holt, J. B., Eds.; VCH: New York, 1990; p 83.

(18) Kushid, B. M.; Likov, A. V. *Int. J. Self-Propag. High-Temp. Synth.* **1992**, *1*, 48.

(19) Kushid, B. M.; Khina, B. B.; Podvoisky, E. P.; Chebotko, I. S. *Combust. Flames* **1994**, *99*, 371.

(20) Varma, A.; Cao, G.; Lebrat, J. P.; Morbidelli, M. *Int. J. Self-Propag. High-Temp. Synth.* **1992**, *1* (1), 9.

(21) Zhang, Y.; Stangle, G. C. *J. Mater. Res.* **1994**, *9*, 2592.

(22) Zhang, Y.; Stangle, G. C. *J. Mater. Res.* **1995**, *10*, 962.

(23) Huque, Z.; Kanury, A. M. *Combust. Sci. Technol.* **1993**, *89*, 27.

(24) Okolovich, E. V.; Merzhanov, A. G.; Khaikin, B. I.; Shkadinskii, K. G. *Dokl. Phys. Chem.* **1977**, *13*, 264.

(25) Logan, K. V.; Sparrow, J. T.; McLemore, W. J. S. In *Combustion and Plasma Synthesis of High-Temperature Materials*; Munir, Z. A., Holt, J. B., Eds.; VCH: New York, 1990; p 219.

(26) Kanury, A. M. *Met. Trans.* **1992**, *23A*, 2349.

(27) Rogachev, A. S.; Varma, A.; Merzhanov, A. G. *Int. J. Self-Propag. High-Temp. Synth.* **1993**, *2* (1), 25.

(28) Pigeon, R. G.; Varma, A. *J. Mater. Sci.* **1993**, *28* (11), 2999.

(29) Vrel, D.; Lihrmann, J. M.; Tobaly, P. *J. Mater. Synth. Process.* **1994**, *2*, 179.

(30) Rogachev, A. S.; Shugaev, V. A.; Kachelmyer, C. R.; Varma, A. *Chem. Eng. Sci.* **1994**, *49* (24B), 4949.

(31) Kachelmyer, C. R.; Rogachev, A. S.; Varma, A. *J. Mater. Res.* **1995**, *10* (9), 2260.

(32) Rogachev, A. S.; Shugaev, V. A.; Khomenko, I.; Varma, A.; Kachelmyer, C. R. *Combust. Sci. Technol.* **1995**, *109* (1−6), 53.

(33) Sundaram, V.; Logan, K. V.; Speyer, R. F. *Ceram. Trans.* **1995**, *56*, 111.

(34) Anselmi Tamburini, U.; Spinolo, G.; Munir, Z. A. *J. Mater. Synth. Process.* **1993**, *1*, 323.

(35) Fromhold, A. T. *J. Phys. Chem. Solids* **1988**, *49*, 1159.

(36) Crank, J. *The Mathematics of Diffusion*; Clarendon Press: Oxford, 1975.

(37) Lapidus, L.; Pinder, G. *Numerical Solution of Partial Differential Equation in Science and Engineering*; John Wiley: New York, 1982.

(38) Press, W. H.; Flannery, B. P.; Teukolsky, S. A.; Vetterling, W. T. *Numerical Recipes*; Cambridge University Press: Cambridge, U.K., 1988.

(39) Pawel, R. E.; Campbel, J. J. *J. Electrochem. Soc.* **1981**, *128*, 1999.

(40) Nekrasov, E. A.; Maksimov, Y. M.; Ziatdinov, M. K.; Shteinberg, A. S. *Combust., Explos. Shock Waves* **1978**, *14*, 575.

(41) Kirdyashkin, A. I.; Maksimov, Y. M.; Merzhanov, A. G. *Combust. Explos. Shock Waves* **1982**, *17*, 591.